The Formation of a "Ghost" Electron Beam via Electron-Ion Trapping at the Gun Test Stand

By Josh Yoskowitz

February 27, 2019

1 Introduction and Discovery of the Ghost Beam

Ion production due to ionization of residual gas generally leads to negative effects on the lifetime and performance of electron accelerators. These effects include photocathode damage and quantum efficiency (QE) degredation due to ion back-bombardment [1, 2], fast ion instabilities, especially in storage rings [3, 4], and ion trapping within the electron beam, which leads to charge neutralization and beam loss [5]. There is extensive and ongoing research on reducing these effects through ion clearing techniques such as introducing clearing electrodes [6] to the beamline and clearing gaps [7] in the electron beam.

The measurement of ion production has only been done in indirect ways, such as measuring the current on an ion precipitator or clearing electrode, where in these cases, only the number of ions can be deduced, not their identity. A recent discovery during an experiment at the Gun Test Stand (GTS) may lead to a method of measuring ion production and characterizing the kinds of ions produced in electron accelerators. On 11/20/18, we ran a 100µA electron beam for 10 minutes at the Gun Test Stand (GTS) (shown below in Figure 1) with the parameters and dimensions listed in Table 1. Note that the cathode and anode are within the gun chamber. After the 10 minute run, the electron beam was shut off and a YAG screen was immediately inserted downstream of the 2nd solenoid lens. A low intensity 100keV electron beam (i.e. with a nominal current on the order of a few nA) was clearly present on the YAG screen, even though the incident laser on the photocathode was off! This "ghost beam" has been observed to only exist while the gun solenoid is on and only after a prior electron beam run. The ghost beam is also long lasting; it has been shown to last for at least several hours.

Gun HV	100kV
Gun Solenoid Current	150A
Anode Bias	+1kV
1st Solenoid Lens Current	0.732A
2nd Solenoid Lens Current	0.723A

Name	Distance from Photocathode (m)
Anode	0.090
Gun Solenoid	0.122
1st Solenoid Lens	0.491
2nd Solenoid Lens	1.017

Table 1: Electron beam & beamline parameters and dimensions

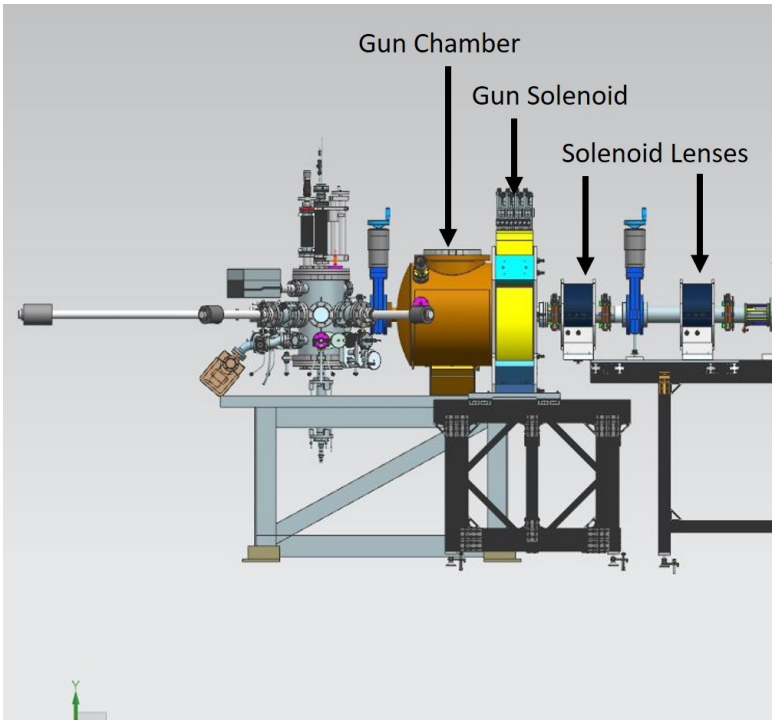

Figure 1: Picture of the front section of the GTS beamline

The currently accepted theory as to why this ghost beam exists and why it is long lasting is the following: the real electron beam ionizes residual gas, creating ions and secondary electrons. After the electron beam is turned off, these ions

and secondary electrons remain trapped within the solenoid lenses via the magnetic mirror effect. Eventually, these ions and secondary electrons recombine and in doing so, emit photons that could reach the photocathode and produce the 100keV electrons that we see on the screen. The hypothesis is that because these 100keV electrons can ionize more residual gas molecules, the ghost beam is self-sustaining. The theory behind these processes is summarized below along with a discussion on the veracity of this hypothesis and a proposal for a future experiment to test this theory.

In the below derivations, since it is difficult to have a consistent notation when using derivations from a collection of articles, each their own notations, I will follow the notation given in the article corresponding to each derivation and define the constants and variables accordingly.

2 Ionization of Residual Gas

While the real electron beam is on, residual gases such as H_2 can be ionized by the high energy electrons. The ion production rate (IPR) depends upon the densities of the residual gas n_g, the density of the electron beam n_e, the ionization cross section σ_g, and the relative velocity of the electron beam $\beta_e c$:

$$\frac{dn_i}{dt} = n_g n_e \sigma_g \beta_e c \tag{1}$$

It is assumed that the electrons are moving much faster than the residual gas molecules such that $\beta_e c$ is essentially the velocity of the electrons.

When ions are formed, they occupy the same volume as the electrons. Thus, $V_g = Al$ where A is the cross sectional area of the beam and l is its length. We can then rewrite eq. (1) as

$$\frac{1}{V_g}\frac{dN_i}{dt} = \frac{d\left(N_i/l\right)}{dt} = n_g \sigma_g \left(n_e A \beta_e c\right) \tag{2}$$

where $\frac{d\left(N_i/l\right)}{dt}$ is the IPR per unit length. The term in parentheses is, by definition, the electron number current I_e/e:

$$\frac{d}{dt}\left(\frac{N_i}{l}\right) = n_g \sigma_g \left(\frac{I_e}{e}\right) \tag{3}$$

Assuming the residual gas is ideal, we can relate n_g to the residual gas pressure and temperature:

$$n_g = \frac{P_g}{k_B T_g} \tag{4}$$

Thus, the IPR per unit length is

$$\frac{d}{dt}\left(\frac{N_i}{l}\right) = \frac{P_g \sigma_g}{k_B T_g}\left(\frac{I_e}{e}\right) \tag{5}$$

The ionization cross section σ_g is derived from Bethe's theory [8, 9]:

$$\sigma_g = \frac{8 a_0^2 \pi I_R A_1}{m_e c^2 \beta_e^2} f\left(\beta_e\right)\left(\ln\frac{2 A_2 m_e c^2 \beta_e^2 \gamma^2}{I_R} - \beta_e^2\right) \tag{6}$$

Numerically, this can be rewritten as:

$$\sigma_g\left(\mathrm{m}^2\right) = \frac{1.872\times10^{-24} A_1}{\beta_e^2} f\left(\beta_e\right)\left[\ln\left(7.515\times10^4 A_2 \beta_e^2 \gamma^2\right) - \beta_e^2\right] \tag{7}$$

$$f\left(\beta_e\right) = \frac{I_i}{T_e}\left(\frac{T_e}{I_i} - 1\right) = \frac{2 I_i}{m_e c^2 \beta_e^2}\left(\frac{m_e c^2 \beta_e^2}{2 I_i} - 1\right) \tag{8}$$

Here, A_1 and A_2 are empirical constants that depend on the gas species, $\gamma = \left(1-\beta_e^2\right)^{-\frac{1}{2}}$ is the Lorentz factor, I_i is the ionization energy, and T_e is the electron kinetic energy. Note that although eq. (5) does not explicitly contain the beam energy, it is taken into account in the ionization cross section.

To get a sense of magnitude, assume that the residual gas is made up of purely hydrogen gas molecules. Below are log-log plots of ionization cross section σ_g vs. beam energy T_e and ion production rate per unit length $\frac{d}{dt}\left(\frac{N_i}{l}\right)$ vs beam current I_e, assuming a beam energy of 100keV.

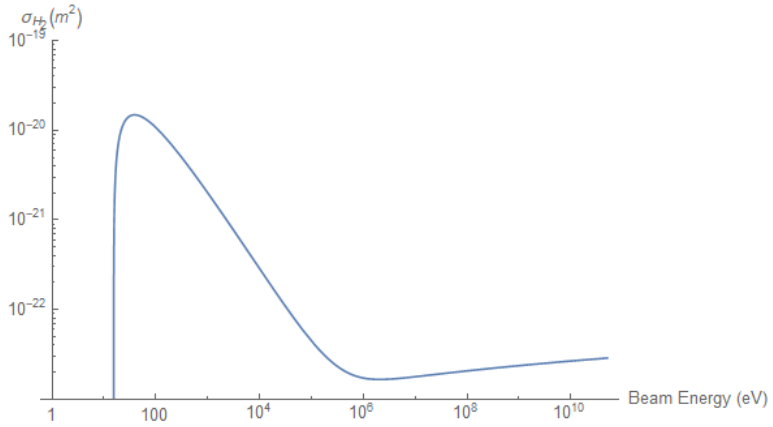

Figure 2: Log-log plot of ionization cross section vs. beam energy for H_2 gas.

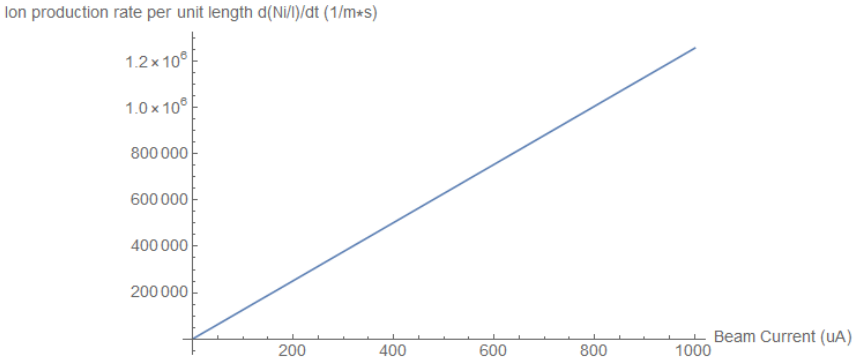

Figure 3: Log-log plot of hydrogen ion production rate per unit length vs beam current for a 100keV electron beam

Using data from the 11/20/18 experiment, the electron beam current is $I = 100\mu A$ and the beam energy was $T_e = 100keV$. The hydrogen gas has a pressure of $P_g = 1.8 \times 10^{-8}$Pa $\left(= 1.3 \times 10^{-10}\text{torr}\right)$ and is assumed to be at room temperature, $T_g = 293.15$K. Using eq. (7), the ionization cross section for hydrogen gas is $\sigma_{H_2} = 4.49\times10^{-23}\text{m}^2$. With $k_B = 1.38\times10^{-23}\frac{\text{J}}{\text{K}}$ and $e = 1.60\times10^{-19}$C, the hydrogen ion production rate per unit length using eq. (5) is $\frac{d}{dt}\left(\frac{N_{H_2^+}}{l}\right) = 1.25\times10^5$ $H_2^+/(\text{m*s})$.

3 Secondary Electron Production and Energy Distribution

When a residual gas molecule is ionized by an electron, an electron is released from the molecule. This ejected electron is called a secondary electron. Note that during the course of ionization, the scattered and ejected electrons are only distinguishable by their kinetic energies. The slower of the two electrons is called the secondary electron. The faster electron is called the primary electron. A diagram showing the ionization process with the trajectories of the incident, scattered, and secondary electrons is shown below in Figure 4.

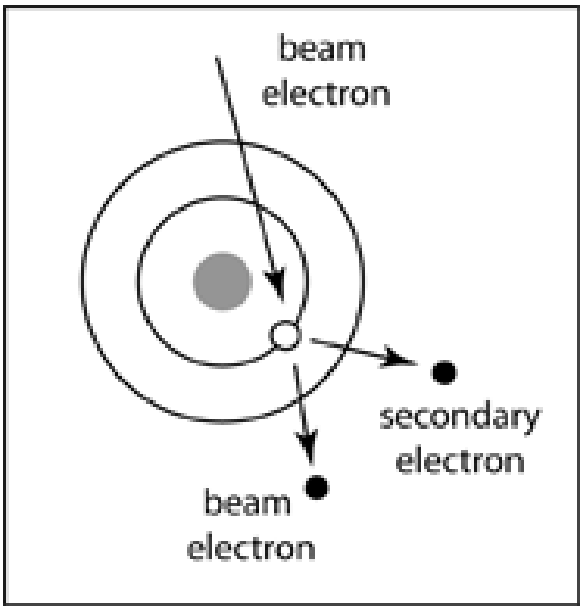

Figure 4: Diagram of the ionization process [10].

The total ionization process can be described by a triply differential cross section $d^3\sigma/dWd\Omega_s d\Omega_p$ where W is the secondary electron energy and Ω_s and Ω_p are the solid angles of the secondary and primary electrons respectively. In order to determine the energy distribution of secondary electrons, given by the singly differential cross section (SDCS) $\frac{d\sigma}{dW}$, one must integrate the triply differential cross section over Ω_s and Ω_p. The total ionization cross section σ_i is thus obtained by integrating over all secondary electron energies W [11]:

$$\frac{d\sigma}{dW} = \iint \frac{d^3\sigma}{dWd\Omega_s d\Omega_p} d\Omega_s d\Omega_p \tag{9}$$

$$\sigma_i = \int \frac{d\sigma}{dW} dW \tag{10}$$

Let T be the incident electron energy, B be the binding energy of the secondary electron, and $U = \langle \vec{p}^2 \rangle / 2m$ be the average kinetic energy of electrons in the subshell (from which the secondary electron was ejected). Note that $T \geq B + W$. We can define energy ratios t, w and u by

$$t = \frac{T}{B}$$
$$w = \frac{W}{B}$$
$$u = \frac{U}{B}$$

Using these definitions, the SDCS in the Binary Encounter Dipole model is

$$\frac{d\sigma}{dW}(T,W) = \frac{4\pi a_0^2 R^2 N}{B^3(t+u+1)} \left[\frac{1}{(w+1)^2} + \frac{1}{(t-w)^2} - \frac{1}{(w+1)(t-w)} + \frac{4u}{3}\left(\frac{1}{(w+1)^3} + \frac{1}{(t-w)^3} \right) \right] \tag{11}$$

where $R = 13.6\text{eV}$ is the Rydberg energy, a_0 is the Bohr radius, and N is the number of electrons in the orbital [11]. We can rewrite eq. (11) as a series

$$\frac{d\sigma}{dW}(T,W) = \frac{4\pi a_0^2 R^2 N}{B^3(t+u+1)} \sum_{n=1}^{3} F_n(t) \left[\frac{1}{(w+1)^n} + \frac{1}{(t-w)^n} \right] \tag{12}$$

After choosing appropriate choices for $F_n(t)$, we have

$$\frac{d\sigma}{dW}(T,W) = \frac{4\pi a_0^2 R^2 N}{B^3(t+u+1)}\left[\frac{(N_i/N)-2}{t+1}\left(\frac{1}{w+1}+\frac{1}{t-w}\right)\right.$$
$$\left.+\left(2-\frac{N_i}{N}\right)\left[\frac{1}{(w+1)^2}+\frac{1}{(t-w)^2}\right]+\frac{\ln t}{N(w+1)}\frac{df}{dw}\right] \tag{13}$$
$$N_i \equiv \int_0^\infty \frac{df(w)}{dw}dw$$

where the term $\frac{df}{dw}$ comes from determining $F_3(t)$ in the asymptotic case of $t \gg w$. Using values for B, U, N, and $\frac{df}{dw}$ for H_2 gas given in Ref. [12], we can plot $\frac{d\sigma}{dW}$ (eq. (13)) as a function of secondary electron energy W (i.e. the energy distribution of secondary electrons) for an incident electron energy of $T = 100\text{keV}$, as shown in Figure 5.

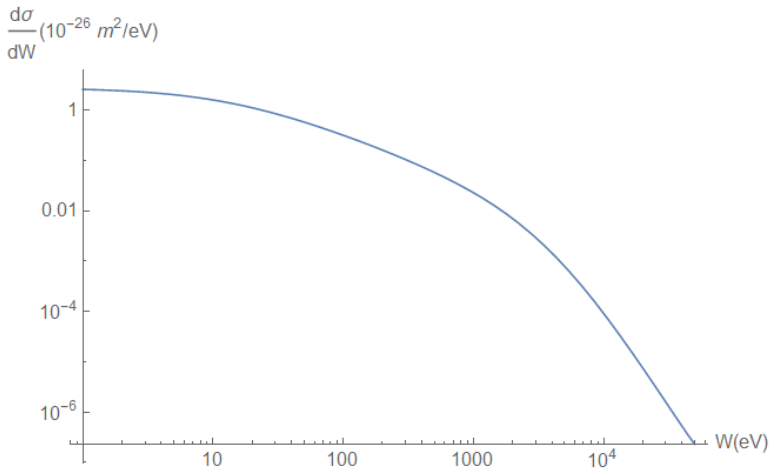

Figure 5: Log-Log Plot of the SDCS $\frac{d\sigma}{dW}$ as a function of W, for $T = 100\text{keV}$ using eq. (13).

4 Electron-Ion Trapping via the Magnetic Mirror Effect

4.1 Magnetic field map

A plot of the longitudinal z-component of the magnetic field of the gun solenoid as a function of z is shown below in Figure 6 using magnetic field maps of the gun solenoid and solenoid lenses with their respective strengths from Table 1.

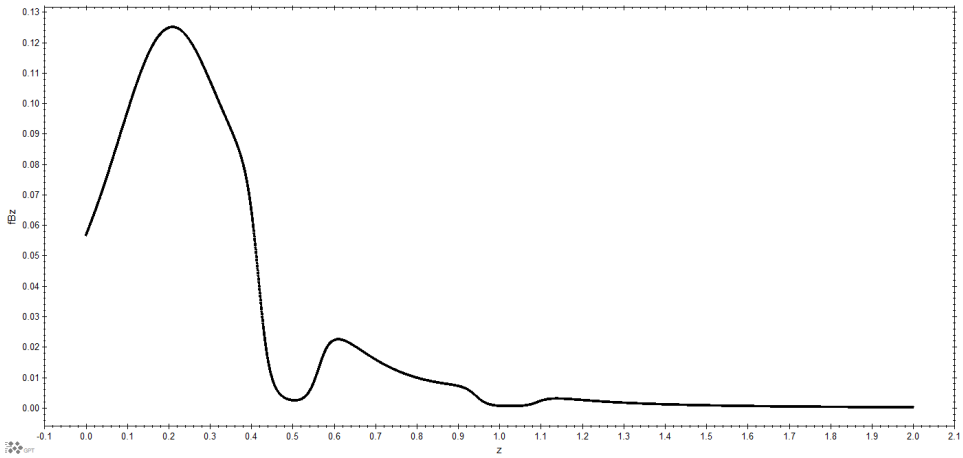

Figure 6: The z-component of magnetic field experienced by electrons along the central axis of the accelerator. The y-axis is in Tesla and the x-axis is in meters.

The longitudinal magnetic field is clearly dominated by the field from the gun solenoid. The two dips at $z \approx 0.5$m and $z \approx 1$m reflect the solenoid lenses having steel shielding that absorbs magnetic fields due to its high permeability. Note that even though the solenoid lenses have non-zero current, the fields produced by these solenoids is negligible. Electrons and ions with sufficiently low energy can be trapped within these magnetic "wells" via the magnetic mirror effect due to the sharp gradients in magnetic field at either end of the wells, as explained below.

4.2 Magnetic Mirror Effect

Charged particles in the presence of a uniform longitudinal magnetic field that is axially symmetric will circulate about the central axis at the Larmor radius:

$$r_L = \frac{mv_\perp}{qB} \tag{14}$$

where$m$ and q are the mass and charge the particle, B is the magnetic field strength and $v_\perp$ is the orbital velocity. The particle also has a magnetic moment μ:

$$\mu = \frac{1}{2}\frac{mv_\perp^2}{B} \tag{15}$$

It can be shown that the magnetic moment μ is an invariant of the motion [13]. Thus, if the uniform longitudinal magnetic field were increasing or decreasing linearly in z (but still uniform transversely), then the transverse velocity $v_\perp$ of a charged particle approaching higher magnetic field will increase. Since the magnetic field cannot perform work, the energy of the particle must be constant. Breaking out the kinetic energy of the particle into its transverse and parallel (to the magnetic field) components:

$$\frac{dE}{dt} = \frac{d}{dt}\left(\frac{1}{2}mv_\perp^2 + \frac{1}{2}mv_\parallel^2\right) = 0 \tag{16}$$

Thus, if $v_\perp$ increases, $v_\parallel$ must decrease and the electron slows down in z. So long as the magnetic field is of sufficient strength, the electron will eventually reflect off of the magnetic field and mirror. We can define a pitch angle, given by $\sin\theta = \frac{v_\perp}{v}$, above which the electron will always mirror. Using the invariance of μ, the threshold pitch angle θ is given by

$$\sin^2\theta_m = \frac{B_1}{B_2} \tag{17}$$

where B_2 is the maximum magnetic field with $B_2 > B_1$ and $\theta \in [0°, 90°]$ [13]. So long as $\theta > \theta_m$, the electron will always mirror. If two solenoids are set up such that θ is above both threshold pitch angles, then the electron is trapped between them. Note that these traps are, in general, *not* stable, as we have neglected coulomb interactions, which can either bring electrons into or knock electrons out of the threshold for mirroring. For a complete derivation of these equations, see Appendix on page 11.

4.3 Thresholds for Trapping

To get a sense of the magnitude of the traps (i.e. how high the "walls" of the trap are), lets plug in numbers using the magnetic field map shown in Figure 6. At lens 1, located at $z \approx 0.5$, the z-component of magnetic field is $B_{0.5} \approx 2.7 \times 10^{-3}$T. The upstream magnetic field maximum, located at $z \approx 0.21$m, is $B_{0.21} \approx 0.13$T. The downstream maximum, located at $z \approx 0.61$m is $B_{0.61} \approx 2.3 \times 10^{-2}$T. At lens 2, located at $z \approx 1.03$m, the magnetic field is $B_{1.03} \approx 7.8 \times 10^{-4}$T. The downstream maximum magnetic field at $z \approx 1.13$m is $B_{1.13} \approx 3.2 \times 10^{-3}$T and the upstream maximum magnetic field at $z \approx 0.9$m is $B_{0.9} = 7.4 \times 10^{-3}$T. It is important to note that the magnetic field wells at the solenoid lenses are not due to the lenses themselves, but rather due to the steel shielding surrounding the lenses, which sharply lowers the magnetic field at the edges of the solenoid lenses. The net magnetic field contributions from the solenoid lenses themselves are negligible compared to that of the gun solenoid.

The threshold pitch angle for each side of both wells is given by eq. (17). However, it is easier to think in terms of particle kinetic energy T rather than pitch angle θ, thus we can derive an equation for T in terms of θ. However, a pitch angle does not uniquely define T. Instead, we can derive a range of kinetic energies using the fact that a particle cannot have a larger Larmor radius than the radius of the beam pipe $R = 0.034$m. The maximum transverse velocity would be the transverse velocity when the Larmor radius equals the beam pipe radius at the center of the well:

$$v_{\perp,max} = \frac{qB_{0.5}R}{m} \tag{18}$$

The velocity of the particle is given by $v = \dfrac{v_\perp}{\sin\theta}$ and so the maximum kinetic energy is $T_{max} = (\gamma - 1)\, mc^2$ where $\gamma = \left(1 - \dfrac{v^2}{c^2}\right)^{-\frac{1}{2}}$. From these equations, we can tabulate the threshold pitch angles and maximum kinetic energies for electrons and H_2^+ ions below in Table 2.

	Electrons/H_2^+ ions		Electrons	H_2^+ ions
Threshold θ for Lens 1, upstream ($B_{0.5} \to B_{0.21}$)	8.29°	T_{th} for Lens 1, upstream ($B_{0.5} \to B_{0.21}$)	39.9keV	9.725eV
Threshold θ for Lens 1, downstream ($B_{0.5} \to B_{0.61}$)	20.0°	T_{th} for Lens 1, downstream ($B_{0.5} \to B_{0.61}$)	6.5keV	1.713eV
Threshold θ for Lens 2, upstream ($B_{1.03} \to B_{0.9}$)	19.0°	T_{th} for Lens 2, upstream ($B_{1.03} \to B_{0.9}$)	582eV	0.159eV
Threshold θ for Lens 2, downstream ($B_{1.03} \to B_{1.13}$)	30.0°	T_{th} for Lens 2, downstream ($B_{1.03} \to B_{1.13}$)	248eV	0.0675eV

Table 2: Threshold pitch angles θ and maximum kinetic energies T for electrons and H_2^+ ions at each solenoid lens

There are two important notes to keep in mind regarding Table 2. First, note that the upstream maximum for lens 2 at $z \approx 0.9$m is not really a maximum, as the magnetic field is higher upstream of $z = 0.9$m. Thus, electrons with certain pitch angles at the center of lens 2 moving towards lens 1 may pass $z = 0.9$m before turning around. These electrons would have a smaller Larmor radius than those that turn around at $z = 0.9$m. Also, note that the maximum of all T_{max} calculations above is 39.9keV, meaning that nowhere can 100keV electrons from the real electron beam or the ghost electron beam get trapped within the solenoid lenses. Thus, electrons that get trapped must be either ions or secondary electrons.

5 Radiative Recombination

5.1 Radiative Recombination Cross Section

When electrons and ions are within close proximity of each other and have low relative velocities, there is a probability that the electron can recombine with the positive ion and emit a photon in a process known as radiative recombination, which can be described by the following process :

$$A^{Z+} + e^- \to A^{(Z-1)+}(n,l) + \gamma \tag{19}$$

where the incident electron e^- recombines with a bare ion A^{Z+} into an orbital vacancy(n,l) and in doing so, loses energy in the form of a photon γ. The energy of the photon is $E_\gamma = E + E_{nl}$ where E is the energy of the incident electron and E_{nl} is the energy of an electron in A in the nl state. In other words, all excess energy in the recombination is taken up by the

photon in RR. The RR cross section formula as a function of E for a recombining electron entering state n given by Kramers is [14]

$$\sigma_n^K(E) = \frac{32\pi}{3\sqrt{3}}\alpha^3 a_0^2 \frac{Z^4 E_0^2}{nE\left(n^2E + Z^2E_0\right)} \tag{20}$$

Here, α is the fine structure constant, a_0 is the Bohr radius, E_0 is the Rydberg constant, and Z is the atomic number of the target atom. Note that $\frac{32\pi}{3\sqrt{3}}\alpha^3 a_0^2 \approx 210.5$ barn. The total recombination cross section is given by summing σ_n over all possible states:

$$\sigma_{tot}(E) = \sum_{n=1}^{\infty} \sigma_n(E) \tag{21}$$

In the case that $E \ll Z^2E_0$ (i.e. the electrons have energies on the order of a few eV or less), we can write $\sigma_{tot}(E)$ explicitly:

$$\sigma_{tot}(E) = \frac{32\pi}{3\sqrt{3}}\alpha^3 a_0^2 \xi^2 \left[b_0 + \ln\xi + b_1/\xi^{2/3} + b_2/\xi^{4/3} + \left(b_3 - b_4\ln\xi\right)/\xi^2\right] \tag{22}$$

where $\xi = \left(Z^2E_0/E\right)^{1/2}$ and $b_0 = 0.161$, $b_1 = 0.518$, $b_2 = 0.074$, $b_3 = 0.068$, and $b_4 = 0.046$. The condition that $E \ll Z^2E_0$ is true in our case of trapped ions recombining with secondary electrons, which have energies on the order of a few eV.

Pajeck and Schuch [14] derived a similar formula for the total RR cross section for low energy electrons ($E \ll E_{nl}$):

$$\sigma_{tot}(E) = \frac{32\pi}{3\sqrt{3}}\alpha^3 a_0^2 \left(Z^2E_0/E\right)\left[\gamma - s(n_{max}) + \ln\left(Z^2E_0/E\right)^{1/2}\right] \tag{23}$$

where $\gamma \approx 0.577$ is the Euler constant (not to be confused with the photon γ from eq. (19)) and $s(n_{max}) = \sum_{n=1}^{n_{max}} \frac{1-g(n)}{n}$. Values for $g(n)$ are given in [14] for different values of n. For H_2 gas, $n_{max} = 2$. Below in Figure 7 is a log-log plot of σ_{tot} as a function of E for electrons recombining with H_2^+ ions.

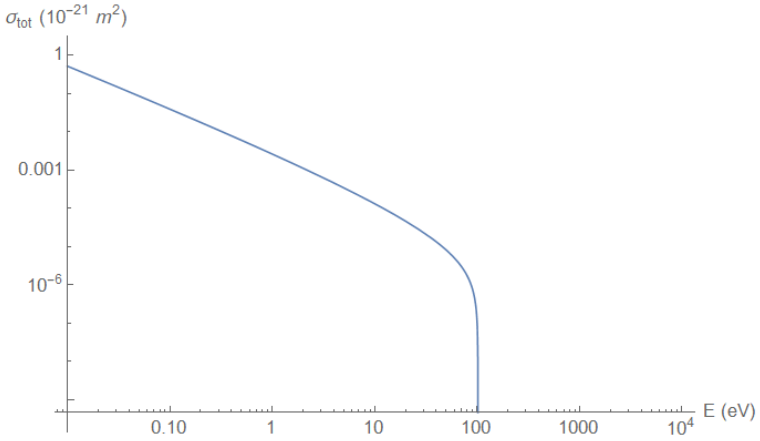

Figure 7: Log-log plot of $\sigma_{tot}(E)$ as a function of E for recombination with H_2^+ ions

5.2 Radiative Recombination Rate

The total radiative recombination rate, α_{tot} is the average of the product of the total RR cross section mutiplied by the relative electron velocity for a given electron velocity distribution f:

$$\alpha_{tot} = \int v\sigma_{tot}(v)\, f(\vec{v})\, d^3v \tag{24}$$

where $\vec{v} = \left(v_\parallel, v_\perp\right)$. Assuming a Maxwellian distribution of electron velocities of the form

$$f(\vec{v}) = \frac{(m/2\pi)^{3/2}}{kT_\perp\left(kT_\parallel\right)^{1/2}} \exp\left(-\frac{mv_\perp^2}{2kT_\perp} - \frac{mv_\parallel^2}{2kT_\parallel}\right) \tag{25}$$

where m is the electron mass (really the electron rest mass energy $m_e c^2$) and $kT_\parallel$ and $kT_\perp$ are electron temperatures in the longitudinal and transverse directions respectively, plugging in eqs. (23) and (25) into (24) and integrating yields [14]

$$\alpha_{tot} = \alpha_0 Z^2 \left(\frac{E_0}{kT_\perp}\right)^{\frac{1}{2}} \left[\frac{3}{2}\gamma - s\left(n_{max}\right) + \ln\left(Z^2 E_0/kT_\perp\right)^{1/2} + D\left(t\right)\right] G\left(t\right) \tag{26}$$

$$\alpha_0 = \left(\frac{32\pi}{3\sqrt{3}}\right)\alpha^3 a_0^2 \times 4\sqrt{\frac{E_0}{2\pi m_e}}$$

$$G\left(t\right) = \sqrt{\frac{t+1}{t}}\arctan\left(\sqrt{t}\right)$$

$$D\left(t\right) = \frac{1}{\arctan\sqrt{t}}\int_0^{\sqrt{t}} \frac{\ln\left(1+z^2\right)}{1+z^2}dz$$

$$t = \frac{kT_\perp - kT_\parallel}{kT_\parallel}$$

Note that eq. (26) tacitly assumes that the recombining electron energy is much smaller than the binding energy (i.e. $E \ll E_{nl}$). In the case of H_2 and considering Figure 5, this assumption is valid. Below in Figure 8 is a plot of α_{tot} as a function of electron temperature $kT_\perp$.

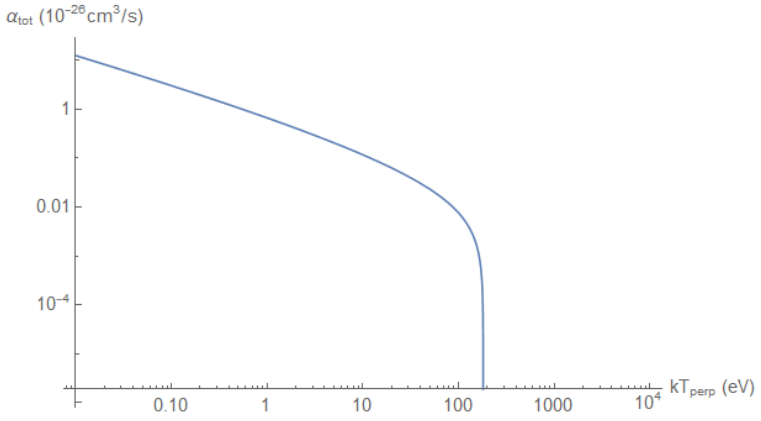

Figure 8: Log-log plot of α_{tot} vs. $kT_\perp$

6 Discussion, Future Work, and Connection to Thesis

From the above calculations, we see that the question is not about whether the ghost beam *exists*. The question is really about *how long* the ghost beam lasts and can it be *self-sustaining*. However, in order to determine how long the ghost beam lasts, we would have to integrate all of these processes (i.e. the ionization cross section and rate, secondary electron differential cross section, and the recombination cross section and rate) for each electron-ion pair and iterate over time until the ghost beam disappears. This integration would be impractical to do analytically, since each of the processes is correlated and depends on the densities of the electrons, ions, and residual gas molecules *at a given time*. Also, there are many different ionization and recombination reaction channels that electrons and ions can take. That is, depending on the atom, there are many different ways that an electron can be ejected from or recombine into an atom and each way has its own cross section. Thus, in order to determine the lifetime of the ghost beam, we can use a simulation package such as GPT or IBSimu to simulate these processes, iterate them over time, and record the lifetime of the ghost beam.

In order to test this theory, two viewports will be added to the part of the beamline within the gun solenoid, shown below in Figure 9. Note that the gun solenoid, which is not shown in either diagram, surrounds the spool (refer to Figure 1). The angled viewport will look for light emission due to recombination of electrons and ions trapped due to the E-field of the anode and B-field of the gun solenoid. The second, perpendicular viewport will be used to look for light in an artificial trap. That is, we can surround the perpendicular viewport with steel shielding, which will absorb the magnetic field from the

gun solenoid and create a magnetic well, like the steel shielding surrounding the solenoid lenses. We were unable to install a viewport that could measure potential light emission within either of the two solenoid lenses.

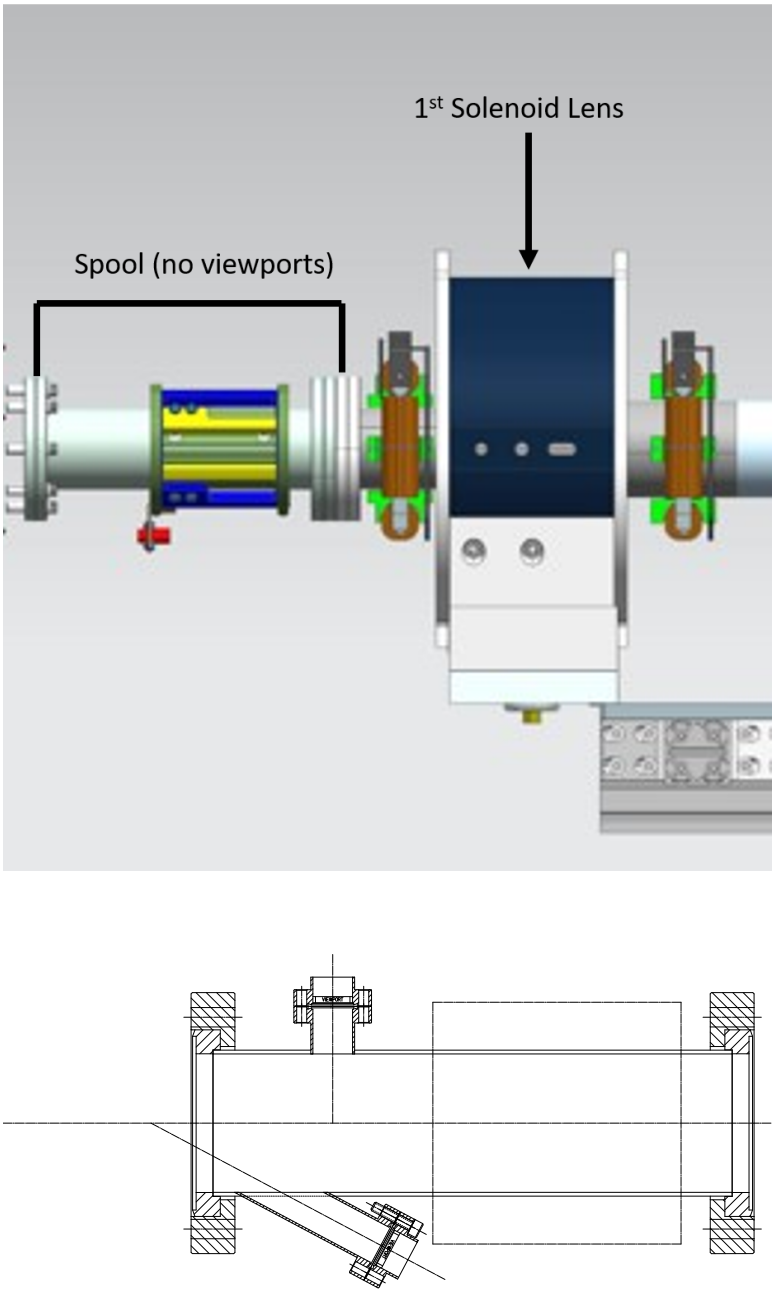

Figure 9: Diagram of location of spool (without viewports) relative to the first solenoid lens (above) and a schematic showing the locations of the two viewports on the spool (below).

Once the viewports are added, we can measure the intensity and wavelength of light emission using a spectral analyzer (or similar device). Any measured light would indicate that there are ions and electrons recombining and the wavelength of the measured light will be characteristic of the identity of the ion, as every atom has characteristic spectral lines associated

with it. Even more, it would add evidence that ions *do* exist in the accelerator, which would help support the theory of ions damaging of the photocathode via ion back-bombardment. In a sense, measuring light from the ghost beam can be an indirect way of measuring ion production in an accelerator. In my thesis, I will be studying the mitigation of the harmful effects of ion production, such as ion back-bombardment of a photocathode, at CEBAF.

References

[1] J. Grames, P. Adderley, J. Brittian, D. Charles, J. Clark, J. Hansknecht, M. Poelker, M. Stutzman, and K. Surles-Law. Ion back bombardment of GaAs photocathodes inside dc high voltage electron guns. In *Proceedings of the 2005 Particle Accelerator Conference*, pages 2875–2877, May 2005. doi: 10.1109/PAC.2005.1591299.

[2] J. Grames, P. Adderley, J. Brittian, J. Clark, J. Hansknecht, D. Machie, M. Poelker, E. Pozdeyev, M. Stutzman, and K. Surles-Law. A biased anode to suppress ion back-bombardment in a dc high voltage photoelectron gun. *AIP Conference Proceedings*, 980(1):110–117, 2008. doi: 10.1063/1.2888075.

[3] Alex W. Chao. Lecture notes on topics in accelerator physics. Technical report, nov 2002.

[4] Avishek Chatterjee, Kelvin Blaser, Michael Ehrlichman, David Rubin, and James Shanks. Fast ion instability at cesr-ta. *Proceedings of the 5th Int. Particle Accelerator Conf.*, IPAC2014:Germany–, 2014. doi: 10.18429/jacow-ipac2014-tupri036.

[5] Yves Baconnier. Neutralization of accelerator beams by ionization of the residual gas, 1985.

[6] Steven Full, Adam Bartnik, Ivan Bazarov, John Dobbins, Bruce Dunham, and Georg Hoffstaetter. Detection and clearing of trapped ions in the high current cornell photoinjector. August 2015. doi: 10.1103/PhysRevAccelBeams.19.034201.

[7] Gisela Pöplau, Ursula van Rienen, and Atoosa Meseck. Numerical studies of the behavior of ionized residual gas in an energy recovering linac. *Physical Review Special Topics - Accelerators and Beams*, 18(4), apr 2015. doi: 10.1103/physrevstab.18.044401.

[8] H. Bethe. Zur theorie des durchgangs schneller korpuskularstrahlen durch materie. *Annalen der Physik*, 397(3):325–400, 1930. doi: 10.1002/andp.19303970303.

[9] Martin Reiser. *Theory and Design of Charged Particle Beams*. Wiley VCH Verlag GmbH, 2008. ISBN 3527407413.

[10] McSwiggen & Associates. What are secondary electrons, how are they formed, and what can they tell us about the sample? Technical report, 2005.

[11] Yong-Ki Kim and M. Eugene Rudd. Binary-encounter-dipole model for electron-impact ionization. *Physical Review A*, 50(5):3954–3967, nov 1994. doi: 10.1103/physreva.50.3954.

[12] Ratko Janev, editor. *Atomic and Molecular Processes in Fusion Edge Plasmas*. Springer US, 1 edition, 1995. ISBN 0-306-45043-7.

[13] Peter T. Gallager. Introduction to plasma physics: Magnetic mirroring. 2013.

[14] M. Pajek and R. Schuch. Total radiative recombination rates for ions interacting with electrons from an electron cooler. *Nuclear Instruments and Methods in Physics Research Section B: Beam Interactions with Materials and Atoms*, 93(3): 241–248, aug 1994. doi: 10.1016/0168-583x(94)95469-0.

7 Appendix: Magnetic Mirror Effect

Following a lecture by Peter Gallager [13], suppose we have a charged particle in a relatively uniform magnetic field that varies in magnitude with z, as is the case with two coaxial solenoids. In cylindrical coordinates we can write the components of the magnetic field:

$$\vec{B} = B_r\hat{r} + B_\theta\hat{\theta} + B_z\hat{z} \tag{27}$$

In the case of coaxial solenoids, $\vec{B}$ has azimuthal symmetry, thus $B_\theta = 0$. From $\nabla \cdot \vec{B} = 0$, we can obtain B_r:

$$\begin{aligned} \nabla \cdot \vec{B} &= 0 \\ \frac{1}{r}\frac{\partial}{\partial r}(rB_r) + \frac{\partial B_z}{\partial z} &= 0 \\ \frac{\partial}{\partial r}(rB_r) &= -r\frac{\partial B_z}{\partial z} \\ rB_r &= -\int_0^r r' \frac{\partial B_z}{dz} dr' \end{aligned}$$

If we assume that $\dfrac{\partial B_z}{\partial z}$ is known at $r = 0$ and does not vary significantly with r (a valid assumption in our case), then

$$\begin{aligned} rB_r &\approx -\frac{1}{2}r^2 \left[\frac{\partial B_z}{\partial z}\right]_{r=0} \\ B_r &= -\frac{r}{2}\left[\frac{\partial B_z}{\partial z}\right]_{r=0} \end{aligned} \tag{28}$$

Now, in the absence of electric fields, the Lorentz force is

$$\begin{aligned} \vec{F}_B &= q\vec{v} \times \vec{B} \\ &= q\left[(v_\theta B_z - v_z B_\theta)\,\hat{r} - (v_r B_z - v_z B_r)\,\hat{\theta} + (v_r B_\theta - v_\theta B_r)\,\hat{z}\right] \end{aligned}$$

Since $B_\theta = 0$,

$$\vec{F}_B = q\left[v_\theta B_z \hat{r} + (v_z B_r - v_r B_z)\,\hat{\theta} - v_\theta B_r \hat{z}\right] \tag{29}$$

For the magnetic mirror, we are mainly concerned with F_z. Using (28), we have:

$$\begin{aligned} F_z &= -qv_\theta B_r \\ &= \frac{qrv_\theta}{2}\frac{\partial B_z}{\partial z} \end{aligned}$$

Averaging over one Larmor period, we have

$$F_{z,avg} = \pm\frac{qr_L v_\perp}{2}\frac{\partial B_z}{\partial z}$$

where $r_L = \dfrac{mv_\perp}{|q|\,B}$ is the Larmor radius. Plugging this in:

$$F_{z,avg} = -\frac{1}{2}\frac{mv_\perp^2}{B}\frac{\partial B_z}{\partial z}$$

But $\dfrac{1}{2}\dfrac{mv_\perp^2}{B} = \mu$, which is the magnetic moment of the particle. Thus,

$$F_{z,avg} = -\mu\frac{\partial B_z}{\partial z} \tag{30}$$

Equation (30) is the "mirror force". If we consider a line element ds along B, then we can extend $F_{z,avg}$ into 3D:

$$F_\parallel = -\mu\frac{dB_z}{ds} = -\mu\nabla_\parallel B$$

$F_\parallel$ is the mirror force parallel to B. Now,

$$\begin{aligned} F_\parallel = m\frac{dv_\parallel}{dt} &= -\mu\frac{dB}{ds} \\ mv_\parallel\frac{dv_\parallel}{dt} &= -\mu v_\parallel\frac{dB}{ds} \end{aligned}$$

Now, $\frac{d}{dt}\left(\frac{1}{2}mv_\parallel^2\right) = \frac{m}{2}\frac{d}{dt}\left(v_\parallel^2\right) = \frac{m}{2}\left(2v_\parallel\frac{dv_\parallel}{dt}\right) = mv_\parallel\frac{dv_\parallel}{dt}$, so

$$\frac{d}{dt}\left(\frac{1}{2}mv_\parallel^2\right) = -\mu v_\parallel\frac{dB}{ds}$$

Since $v_\parallel = \frac{ds}{dt}$,

$$\frac{d}{dt}\left(\frac{1}{2}mv_\parallel^2\right) = -\mu\frac{ds}{dt}\frac{dB}{ds} = -\mu\frac{dB}{dt}$$

Since the particle's energy is conserved in the absence of electric fields, $\frac{dE}{dt} = \frac{d}{dt}\left(\frac{1}{2}mv_\parallel^2 + \frac{1}{2}mv_\perp^2\right) = \frac{d}{dt}\left(\frac{1}{2}mv_\parallel^2 + \mu B\right) = 0 \rightarrow \frac{d}{dt}\left(\frac{1}{2}mv_\parallel^2\right) = -\frac{d}{dt}(\mu B)$. Thus,

$$\begin{aligned}
\mu\frac{dB}{dt} - \frac{d(\mu B)}{dt} &= 0 \\
\mu\frac{dB}{dt} - \left(B\frac{d\mu}{dt} + \mu\frac{dB}{dt}\right) &= 0 \\
B\frac{d\mu}{dt} &= 0
\end{aligned} \tag{31}$$

Since $B \neq 0$ by assumption, $\frac{d\mu}{dt} = 0$, so μ is a constant of motion.

Let's apply this to the case of two coaxial solenoids. Suppose we have a charged particle between two coaxial solenoids that are relatively close together. Let the z-axis be the along the central axis of the solenoids with $z = 0$ at their midpoint. At two different locations z_1 and z_2, the strength of the magnetic field is B_1 and B_2 respectively, and the particle has transverse velocities $v_{\perp 1}$ and $v_{\perp 2}$ respectively. (Note that since there is azimuthal symmetry and we assume that the particle is close enough to the axis to feel the effects of the solenoidal magnetic fields, we only need to specify their z-component). Invoking the invariance of μ, we have

$$\begin{aligned}
\mu_1 &= \mu_2 \\
\frac{mv_{\perp 1}^2}{2B_1} &= \frac{mv_{\perp 2}^2}{2B_2} \\
v_{\perp 1}^2 &= v_{\perp 2}^2\frac{B_1}{B_2}
\end{aligned} \tag{32}$$

Also, since $\frac{dE}{dt} = 0$,

$$\begin{aligned}
\frac{d}{dt}\left(\frac{1}{2}mv_\parallel^2 + \frac{1}{2}mv_\perp^2\right) &= 0 \\
\frac{1}{2}mv_\parallel^2 + \frac{1}{2}mv_\perp^2 &= \varepsilon \\
v_\parallel^2 + v_\perp^2 &= \frac{2\varepsilon}{m}
\end{aligned} \tag{33}$$

where ε is a constant. Suppose the particle moves from z_1 to z_2. If $B_1 < B_2$, then in order for equation (32) to be true, $v_{\perp 2} > v_{\perp 1}$, meaning that the particle's transverse velocity *increases*. By equation (33), this means that $v_\parallel$ *decreases* and the particle slows down. Solving (33) for $v_\perp^2$ and inserting it into (32), we have

$$\begin{aligned}
\frac{2\varepsilon}{m} - v_{\parallel 1}^2 &= \left(\frac{2\varepsilon}{m} - v_{\parallel 2}^2\right)\frac{B_1}{B_2} \\
v_{\parallel 1}^2 &= \frac{2\varepsilon}{m} - \left(\frac{2\varepsilon}{m} - v_{\parallel 2}^2\right)\frac{B_1}{B_2} \\
v_{\parallel 1}^2 &= \frac{2\varepsilon}{m}\left(1 - \frac{B_1}{B_2}\right) + v_{\parallel 2}^2\frac{B_1}{B_2}
\end{aligned}$$

The case when $v_{\parallel 2} = 0$ corresponds to the case when the particle's velocity is solely *transverse* at z_2, i.e. the particle has no z-component of velocity. In this case,

$$v_{\parallel 1}^2 = \frac{2\varepsilon}{m}\left(1 - \frac{B_1}{B_2}\right)$$

where $B_1 < B_2$ by assumption so that the r.h.s. is positive. Define $\sin\theta = \frac{v_\perp}{v}$ where θ can be thought of as the pitch angle of the particle. Note that $\theta \in [0°, 90°]$. From (32),Equation (34) denotes the threshold for mirroring.

$$\sin^2\theta = \frac{B_1}{B_2} \tag{34}$$

Particles can mirror so long as $\sin^2\theta \geq \frac{B_1}{B_2}$, i.e. θ is large and $B_2 > B_1$ However, if θ is too small, the particle slows down, but does not mirror. $v_\parallel$ remains constant when $B_2 = B_1$ and increases when $B_2 < B_1$; it cannot decrease to zero.

Define B_m as the maximum magnetic field and R_m as the mirror ratio $R_m = \frac{B_m}{B_1}$. The smallest value that θ can be with a particle mirroring is given by

$$\sin^2\theta_m = \frac{B_1}{B_m} = \frac{1}{R_m} \tag{35}$$

So long as $\theta > \theta_m$, the particle will mirror. Particles with $\theta \leq \theta_m$ escape the mirror.